Journal of Hazardous Materials 366 (2019) 130–139

Contents lists available at ScienceDirect

Journal of Hazardous Materials

journal homepage: www.elsevier.com/locate/jhazmat

Effective removal of inorganic mercury and methylmercury from aqueous solution using novel thiol-functionalized graphene oxide/Fe-Mn composite

Yao Huang[a,b], Yanyan Gong[a,*], Jingchun Tang[b,*], Siyu Xia[b]

[a] School of Environment, Guangdong Key Laboratory of Environmental Pollution and Health, Jinan University, Guangzhou 511443, China
[b] College of Environmental Science and Engineering, Key Laboratory of Pollution Processes and Environmental Criteria (Ministry of Education), Tianjin Engineering Center of Environmental Diagnosis and Contamination Remediation, Nankai University, Tianjin 300350, China

GRAPHICAL ABSTRACT

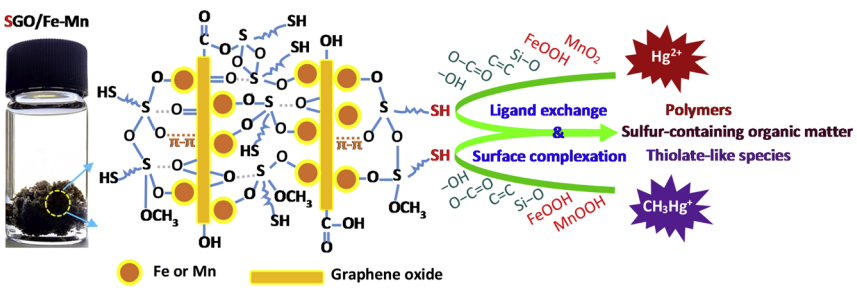

ARTICLE INFO

Keywords:
Mercury
Methylmercury
Sorption
Thiol-functionalized graphene oxide/Fe-Mn
Remediation

ABSTRACT

A novel thiol-functionalized graphene oxide/Fe-Mn (SGO/Fe-Mn) was investigated for aqueous Hg^{2+} and CH_3Hg^+ removal. Mercury were removed mainly through ligand exchange and surface complexation with surface active sites (i.e., −SH, −OH, O−C=O, C=C, Si−O, and π−π bond). −SH had the strongest binding ability with mercury, forming sulfur-containing organic matter or polymers with Hg^{2+}, and sulfur-containing organometallic compounds or thiolate-like species with CH_3Hg^+. The BET sorption isotherm model well simulated the sorption isotherm data of Hg^{2+} ($R^2 = 0.995$, $q_m = 233.17$ mg/g) and CH_3Hg^+ ($R^2 = 0.997$, $q_m = 36.69$ mg/g), indicating a multilayer adsorption process. The mercury uptake was promoted with the increase of 3-MPTS content, adsorbent dosage, and pH (< 5.5), whereas the uptake was inhibited by high pH (> 5.5) and high concentrations of humic acid and electrolytes. SGO/Fe-Mn demonstrated high mercury uptake in simulated surface water/groundwater and in the presence of Pb, Cu, Ni, Sb, Cd and Zn. The mercury-laden SGO/Fe-Mn can be successfully regenerated and reused for three times with 98.1% and 67.0% of original Hg^{2+} and CH_3Hg^+ sorption capacity when 5% thiourea + 2 M KI was used as the desorbing agent. This study demonstrates potential and viability of SGO/Fe-Mn for mercury remediation.

1. Introduction

Mercury is one of the most persistent and toxic heavy metals in the environment, existing in various species, e.g., Hg°, Hg^+, Hg^{2+}, CH_3Hg^+, and $CH_3CH_2Hg^+$. Hg^{2+} is the most predominant inorganic form of mercury in natural waters and it can bind to the amino acid cysteine in proteins [1]. CH_3Hg^+ is a neurotoxin, posing a potential threat to humans and wildlife due to its persistence and biomagnification over the food chain [2]. Controlling mercury contamination has been a primary objective of local and national health and

* Corresponding authors.
E-mail addresses: yanyangong@jnu.edu.cn (Y. Gong), tangjch@nankai.edu.cn (J. Tang).

https://doi.org/10.1016/j.jhazmat.2018.11.074
Received 11 July 2018; Received in revised form 15 November 2018; Accepted 17 November 2018
Available online 18 November 2018
0304-3894/

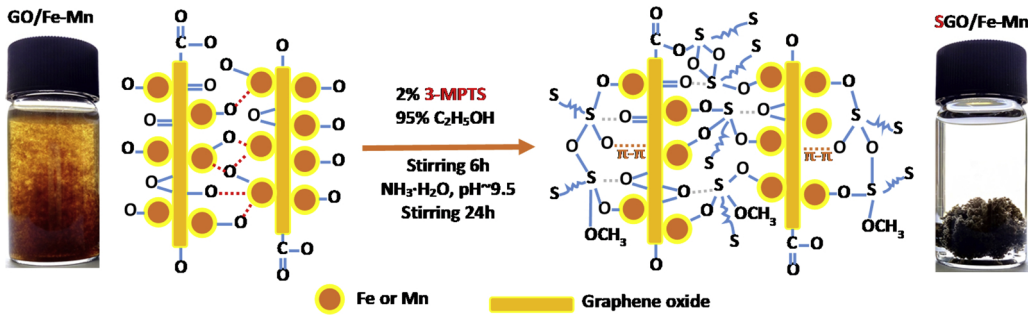

Fig. 1. Preparation of SGO/Fe-Mn.

environmental agendas for decades, and most recently, it has risen to an issue of international concern as addressed by the 2013 Minamata Convention on Mercury.

Adsorption is recognized as one of the most promising approaches for aqueous mercury removal in terms of its low cost, ease of operation, and simplicity of design [3]. Thiol-functionalized adsorbents are expected to exhibit a high adsorption capacity and a strong binding affinity for mercury as a consequence of a soft Lewis acid-base interaction [3–9]. For instance, thiol-incorporated activated carbon derived from fir wood sawdust exhibits a higher maximum adsorption capacity of Hg^{2+} (129 mg/g) than activated carbon (107 mg/g) [6]. And the thiol-functionalized graphene oxide is an effective and highly selective adsorbent for Hg^{2+} with a maximum adsorption capacity of 107.52 mg/g [5]. However, most of the researchers were limited to the removal of Hg^{2+} at initial concentrations of 10–1000 mg/L [3,6,10,11], which are much higher than mercury concentrations relevant to environmental conditions (usually less than 3 mg/L) [12,13]. Moreover, the removal of aqueous organic mercury, in particular, methylmercury, was seldom investigated. Compared with Hg^{2+}, CH_3Hg^+ has weak binding ability to common functional groups (such as hydroxyl, carboxyl, halogen atom, and amino, etc.). Therefore, the adsorption capacity of CH_3Hg^+ was relatively low. Therefore, it is imperative to explore adsorptive materials with high sorption affinity and great sorption capacity for low concentrations of both Hg^{2+} ($\leq$ 3 mg/L) and methylmercury ($\leq$ 50 μg/L).

3-mercaptopropyltrimethoxysilane (3-MPTS) is a widely used thiol-modification chemical [3,9,14–16], and it can carry out hydrolysis and dehydration/ligand exchange with hydroxyl groups on the surface of raw materials (e.g., metal oxides, smectite, and SiO_2) [9,14,15] or form a strong interfacial adhesion with surface oxygen containing groups (e.g., C—O, and carboxyl O=C—O) [16,17]. A novel thiol-functionalized graphene oxide/Fe-Mn (SGO/Fe-Mn) was developed via three different approaches (i.e., acetic acid method, neutral method, and ammonium hydroxide method) in our previous study and their physicochemical properties and CH_3Hg^+ sorption performance were characterized [4]. The SGO/Fe-Mn synthesized using the ammonium hydroxide method demonstrated the most thiol groups, negative charge, sp^3 defects, and FeOOH, thus, highest CH_3Hg^+ maximum sorption capacity. However, detailed investigation into the removal effectiveness of Hg^{2+} and CH_3Hg^+ by SGO/Fe-Mn has been lacking. Furthermore, the influence of factors such as 3-MPTS content, SGO/Fe-Mn dosage, pH, ionic strength, humic acid, and coexisting heavy metals on mercury removal, the removal effectiveness of SGO/Fe-Mn in simulated waters and regeneration have not yet been investigated.

The overall goal of this study was to systematically investigate the removal effectiveness and mechanisms of Hg^{2+} and CH_3Hg^+ by SGO/Fe-Mn from water. The specific objectives were to: (1) prepare and characterize SGO/Fe-Mn before and after mercury adsorption, elucidating the underlying sorption mechanisms; (2) examine the effects of initial mercury concentration, 3-MPTS content, SGO/Fe-Mn dosage, pH, ionic strength, humic acid, and coexisting heavy metals on mercury adsorption; (3) evaluate the desorption and regeneration of the mercury-laden SGO/Fe-Mn; and (4) test the Hg^{2+} removal effectiveness in simulated surface water, groundwater and seawater.

2. Materials and methods

2.1. Chemicals

All chemicals used in this study were of analytical grade or higher. $Hg(NO_3)_2{\cdot}H_2O$ was purchased from Chengdu Aikeda Chemical Technology (Sichuan, China). CH_3HgCl was provided by Dr. Ehrenstorfer GmbH (Augsburg, Germany). 3-MPTS and ethanol were purchased from J&K Scientific (Beijing, China). Graphene oxide, humic acid, thiourea, $FeSO_4{\cdot}7H_2O$, $KMnO_4$, NH_4OH (25% NH_3 in H_2O), HNO_3, NaOH, and KI were procured from Tianjin Chemical Reagent Technology (Tianjin, China).

2.2. Preparation and characterization of SGO/Fe-Mn

SGO/Fe-Mn was prepared following our previously reported approach (Fig. 1) [4,18]. The details are present in the supplementary information (SI).

SGO/Fe-Mn before and after mercury adsorption was characterized. Zeta potential (ζ) was determined using a Malvern Zeta sizer Nano ZEN3690 Instrument (Malvern Instruments, Worcestershire, UK). Fourier transform infrared (FTIR) analysis was conducted by a FTS-6000 spectrometer (Bio-rad, California, USA). Raman spectra was carried out on a Renishaw inVia Raman microscope system (Renishaw, Gloucestershire, UK). Surface elemental composition was analyzed via X-ray photoelectron spectroscopy (XPS) using a PHI-5000 Versaprobe II spectrometer (ULVAC-PHI, Chigasaki, Japan).

2.3. Batch sorption experiments

Hg^{2+} and CH_3Hg^+ sorption tests by SGO/Fe-Mn were carried out in sealed 30 mL PTFE vials. In all cases, 0.01 M $NaNO_3$ was added to simulate real water ionic strength. The pH of the mixture was adjusted to 7.0 ± 0.2 with HNO_3 (1 M and 0.1 M) and NaOH (1 M and 0.1 M). The vials were then sealed and agitated on an end-over-end rotator at 40 rpm for three days at room temperature (25 ± 2 °C). Upon equilibrium, samples were filtered through 0.22 μm PTFE filters, and the filtrates were analyzed for aqueous mercury. Control tests in the absence of the adsorbents showed that the loss of Hg^{2+} and CH_3Hg^+ during the experiments were < 4% for all cases. All experiments were performed in triplicate.

Mercury sorption isotherms were conducted at 15 mg/L SGO/Fe-Mn, and the initial concentrations of Hg^{2+} and CH_3Hg^+ were 0.1–11 mg/L and 0.05–13 mg/L, respectively.

To determine the effect of 3-MPTS content on mercury removal, the SGO/Fe-Mn was prepared at fixed GO and Fe-Mn concentrations (GO: 120 mg/L; Fe-Mn: 21 mg/L) but with various volume fractions of the 3-MPTS in the suspension, namely, 2%, 6%, and 8%. The initial concentration of Hg^{2+} and CH_3Hg^+ were 3 mg/L (15 mg/L SGO/Fe-Mn)

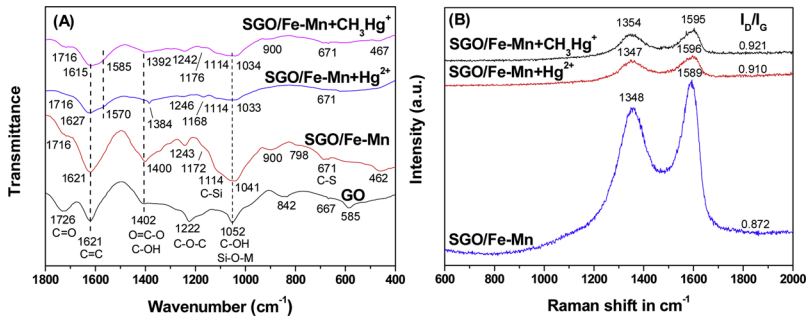

Fig. 2. (A) FTIR spectra and (B) Raman spectra of SGO/Fe-Mn before and after mercury adsorption.

and 50 μg/L (50 mg/L SGO/Fe-Mn), respectively. To test the effect of SGO/Fe-Mn dosage, various concentrations of SGO/Fe-Mn (5–25 mg/L) were obtained with 3 mg/L Hg^{2+}, while 30–70 mg/L SGO/Fe-Mn were mixed with 50 μg/L CH_3Hg^+. To examine the effect of pH, the reaction pH was kept constant at 4–9, respectively. To investigate the ionic strength and humic acid effect, the sorption tests were carried out in the presence of 0-0.1 M $NaNO_3$ and 0–25 mg/L of humic acid, respectively. For comparison, mercury sorption tests via GO/Fe-Mn were conducted under otherwise identical conditions.

2.4. Desorption and regeneration experiments

Potassium iodide (KI) and thiourea were widely used for desorption of mercury-laden adsorbent (e.g., log*K* with Hg^{2+} are 23.8 and 22.1, respectively) [5,10,15]. Five combinations were adopted: 5% thiourea + 2 M KI, 5% thiourea + 4 M KI, 2% thiourea + 4 M KI, 5% thiourea, and 4 M KI. It should be noted that 5% thiourea means 5 g of thiourea in 100 mL of desorption solution.

Before the desorption treatment, the mercury-laden SGO/Fe-Mn were separated (4000 rpm, 10 min) and washed three times with distilled water. Then, 28 mL of regeneration agents were added to the PTFE vials, and the mixture was sealed and agitated on an end-over-end rotator at 40 rpm at room temperature (25 ± 2 °C) for 24 h. The SGO/Fe-Mn was separated by centrifugation (4000 rpm, 10 min) and the mercury concentrations in the supernatant were analyzed. The desorption efficiency was calculated according to the following equation [3]:

$$\textit{Desorption efficiency}\ (\%) = \frac{(C_{ed} - C_0)V_d}{q_e m} \times 100 \quad (1)$$

where C_{ed} is mercury equilibrium concentration (mg/L) in the eluent after desorption, C_0 is the mercury concentration in the eluent before desorption (mg/L), V_d is the volume of the eluent (L), q_e is the mercury adsorption capacity (mg/g) of SGO/Fe-Mn obtained in the adsorption experiment, and m is the mass (g) of SGO/Fe-Mn. The regenerated SGO/Fe-Mn was then reused in another cycle to sorb and desorb mercury, and the sorption-regeneration cycles were repeated three times to investigate the reusability of the material.

2.5. Removal of Hg^{2+} from simulated waters and effects of coexisting heavy metals

In real waters, Hg^{2+} is the major form of mercury, and the bioaccumulation depends upon the formation and uptake of CH_3Hg^+ [19]. Removal of Hg^{2+} from the following three simulated waters via SGO/Fe-Mn were tested: (1) simulated surface water [20]: 6.5 mg/L $NaHCO_3$, 0.58 mg/L KCl, 29.4 mg/L $CaCl_2{\cdot}2H_2O$, and 12.3 mg/L $MgSO_4{\cdot}7H_2O$; (2) simulated groundwater [21]: 292.5 mg/L NaCl, 142 mg/L Na_2SO_4, 88.8 mg/L $CaCl_2$, and 252 mg/L $NaHCO_3$; and (3) simulated sea water [22]: 24,530.0 mg/L NaCl, 5200.0 mg/L $MgCl_2$, 4090.0 mg/L Na_2SO_4, 1160.0 mg/L $CaCl_2$, 695.0 mg/L KCl, 201.0 mg/L $NaHCO_3$, 101.0 mg/L KBr.

To determine the effect of coexisting heavy metals on Hg^{2+} adsorption, the mixture of Pb, Cu, Ni, Sb, Cd and Zn were introduced to the reaction system. The total concentrations of coexisting heavy metals were set at 1 mg/L (each metal was 0.17 mg/L) and 3 mg/L (each metal was 0.5 mg/L), respectively.

The concentration of Hg^{2+} was 3 mg/L, the dosage of SGO/Fe-Mn was 15 mg/L, and the reaction time was 3 days.

2.6. Analytical methods

pH value was measured using a PB-10 pH meter (Sartorius, Gottingen, Germany). Mercury concentration was determined using an AFS-933 atomic fluorescence spectrometer (Titan Instruments, China) following the Environmental Protection Standards of People's Republic of China (HJ 694-2014). The detection limit was 0.04 μg Hg/L. The 3-MPTS content in SGO/Fe-Mn was measured by an EA3000 type organic element analyzer (Euro Vector, Italy). The iron and manganese contents in the SGO/Fe-Mn were measured using a ContrAA 700 continuous light source graphite furnace atomic absorption spectrometer (Analytikjena, Germany). Pb, Cu, Ni, Sb, Cd and Zn concentrations were detected using a NexION 350X inductively coupled plasma-mass spectrometry (PerkinElmer, United States) following the Environmental Protection Standards of People's Republic of China (HJ 700-2014). The detection limits of Pb, Cu, Ni, Sb, Cd and Zn were 0.09, 0.08, 0.06, 0.15, 0.05 and 0.67 μg/L, respectively.

3. Results and discussion

3.1. Characterization of SGO/Fe-Mn before and after mercury sorption

The characteristic stretching frequencies are compared in Fig. 2A and Fig. S1. For SGO/Fe-Mn, the peaks at 1716, 1621, 1400, 1243, 1114, 1041 and 671 cm^{-1} were ascribed to the vibration of C=O, C=C, O=C–O/tertiary C–OH, C–O–C, C–Si, primary C–OH/Si–O–M (M = Si or Metal), and C–S, respectively [4,23]. –SH stretching vibration was weak and broadened at 2600-2550 cm^{-1} [4].

Upon Hg^{2+}/CH_3Hg^+ uptake, the FTIR spectra demonstrated similar absorption bands, while the transmittance of C=O, C=C, O=C–O/tertiary C–OH, C–O–C, C–Si, primary C–OH/Si–O–M (M = Si or Metal), and C–S were significantly reduced. The C=C band shifted from 1621 cm^{-1} to 1627/1615 cm^{-1}, meanwhile, two new peaks at 1570 and 1585 cm^{-1} appeared, which may be ascribed to the π-π interaction between C=C and mercury [24]. The O=C–O/tertiary C–OH band shifted from 1400 cm^{-1} to 1384/1392 cm^{-1}, and primary C–OH/Si–O–M (M = Si or Metal) band shifted from 1041 cm^{-1} to 1033/1034 cm^{-1}, respectively. These changes were attributed to the surface complexation and ligand exchange between SGO/Fe-Mn and mercury.

Raman spectra are depicted in Fig. 2B. Two characteristic peaks of SGO/Fe-Mn at 1348 and 1589 cm^{-1} were observed corresponding to the D-band (structural defects or partially disordered structures of sp^3 domains) and G-band (in-plane vibrational mode of sp^2 domains including sp^2 C=C stretch vibrations) [25]. The surface enhanced Raman

scattering (SERS) enhancement disappeared after mercury sorption, i.e., the intensities of D band and G band decreased by 82%, indicating a reduction in the charge transfer and surface roughness [26,27]. The charge transfer enhancement of graphene oxide composite involves the chemisorption interaction and the metal-adsorbate charge transfer [26]. Our previous study found that the SERS of SGO/Fe-Mn (compared with graphene oxide) was mainly due to the loading of Fe-Mn oxide particles, whereas the modification using 3-MPTS did not affect the SERS [4,18]. This indicated that the loading of metals such as Fe and Mn had a greater influence than organic maters on the charge transfer of graphene oxide composite. Upon mercury sorption, the interactions between mercury and the surface thiol groups as well as Fe-Mn oxide might change the charge transfer between Fe-Mn oxide and graphene oxide and resulted in a reduction in the surface roughness of the SGO/Fe-Mn. D/G band slightly shifted from 1348/1589 cm^{-1} (SGO/Fe-Mn) to 1347/1596 cm^{-1} (SGO/Fe-Mn + Hg^{2+}) and 1354/1595 cm^{-1} (SGO/Fe-Mn + CH_3Hg^+), respectively, which can be ascribed to the change of electronegativity or steric strain upon mercury sorption [28]. Furthermore, the intensity ratios of D and G band (I_D/I_G) for Hg^{2+}- and CH_3Hg^+-laden SGO/Fe-Mn (0.910 and 0.921) were higher than that of SGO/Fe-Mn (0.872), indicating that mercury-laden SGO/Fe-Mn contained more defects and there was a significant increase in disordered carbon due to the interactions between sp^2-type groups (e.g., C=C and O−C=O) and mercury [4,29].

The XPS spectra of C1s, Fe2p, Mn2p, S2p, Si2p, and Hg4f are shown in Fig. 3. XPS wide scan are shown in Fig. S2. For SGO/Fe-Mn, the peaks of C1s (Fig. 3A) at 282.7, 284.1, 286.1, 287.4, and 288.8 eV were ascribed to C−Fe, C−C/C=C, C−O, C=O, and O−C=O, respectively [30,31]. The Fe2p peaks (Fig. 3D) at 707.3, 708.6, 710.0, 711.7, 715.5, 718.7, and 724.2 eV were characteristic of Fe_3C, FeO, Fe_2O_3, FeOOH, Fe^{2+} $2p_{3/2}$ satellite peak, Fe^{3+} $2p_{3/2}$ fingerprint peak, and $Fe2p_{1/2}$, respectively [4,18,32]. The Mn2p peaks (Fig. 3G) at 638.1, 640.3, 641.3, 644.7, 649.6, and 652.3 eV were ascribed to Mn^0, MnO, MnOOH, MnO_2, Mn^{2+} $2p_{3/2}$ satellite peak, and $Mn2p_{1/2}$, respectively [4,32,33]. The S2p binding energies (Fig. 3J) at 163.9, 162.7, 167.6 and 160.2 eV were representative of $S2p_{1/2}$ (C−S), $S2p_{3/2}$ (−SH), oxidized sulfur (e.g., thiosulfate, sulfite) and sulphides (e.g., FeS, Fe_2S_3), respectively [4,34–36]. The Si2p binding energies (Fig. 3M) at 98.9, 101.3, 101.9, and 103.8 eV represented Si(0)/Si−Fe, Si−O−Si, C−O−Si/Si−O−M (M = Si or metal), and SiO_2, respectively [4,34,37].

Upon Hg^{2+}/CH_3Hg^+ sorption (Fig. 3A, B and C), C=O decreased by 4.3%/0.2% (shifted by 0.4/0.6 eV), C−O increased by 1.3%/20.3% (shifted by 0.4/0.6 eV), O−C=O increased by 2.6%/2.8% (shifted by -0.2/0 eV), respectively, which can be attributed to the ligand exchange and surface complexation between SGO/Fe-Mn with mercury. The shift of C=C bond (both 0.7 eV) in Hg^{2+}/CH_3Hg^+-laden SGO/Fe-Mn was attributed to the cation-π bonds between SGO/Fe-Mn and Hg^{2+}/CH_3Hg^+ cations [24]. The decrease of C−C/C=C (20.8%) in CH_3Hg^+-laden SGO/Fe-Mn was mainly due to unsaturated C=C, and the increase of C=C (2.6%) (shifted by 0.7 eV) and decrease of C=O (4.3%) in Hg^{2+}-laden SGO/Fe-Mn may be related to the aldol reaction [38].

FeOOH, FeO, and Fe_2O_3 were reported can form the charge distribution multi-site complexation with mercury, including inner- and outer-sphere complexation (monodentate/ternary) as well as ligand exchange [39]. After Hg^{2+}/CH_3Hg^+ sorption (Fig. 3D, E and F), FeOOH decreased the most (decreased by 22.0%/21.3% and shifted by 0.4/1.6 eV) and Fe_2O_3 increased the most (increased by 9.3%/14.5% and shifted by 0.6/1.2 eV), indicating FeOOH played the most important role among Fe2p, and promoted the formation of Fe_2O_3. The change in FeO (decreased/increased by 0.2%/0.8% and shifted by 1.1/1.6 eV) indicated the presence of redox reaction.

Hydrous manganese oxide (e.g., MnOOH, MnO, and MnO_2) serves as an economic and selective sorbent for mercury, the abundant surface hydroxyls groups act as active sorption sites for mercury binding (ligand exchange and surface complexation) [40,41]. Compared with SGO/Fe-Mn (Fig. 3G, H, I), MnO_2 decreased the most (decreased by 6.6%, shifted by 1.3 eV) after Hg^{2+} sorption, MnOOH decreased the most (decreased by 12.6%, shifted by 1.6 eV) after CH_3Hg^+ sorption, indicating that they played a major role. In addition, the redox reaction was observed. For instance, upon Hg^{2+} uptake, Mn^0 and Mn^{2+} (MnO) decreased by 2.5% and 0.8%, respectively, while Mn^{3+} (MnOOH) increased by 1.8%. Upon CH_3Hg^+ sorption, Mn^0 and Mn^{4+} (MnO_2) decreased by 5.0% and 9.6%, respectively, while Mn^{2+} (MnO) increased by 19.5%.

After Hg^{2+} sorption (Fig. 3J, K), there were two new bands at 174.8 and 171.6 eV, which were ascribed to S satellite lines of sulfur-containing organic matter or polymers, e.g., $(-C_6H_4S-)_n$ [42]. After CH_3Hg^+ sorption (Fig. 3J, L), two new characteristic peaks at 165.4 and 162.0 eV were representative of sulfur-containing organometallic compounds and thiolate-like species [43,44]. For Hg^{2+}- and CH_3Hg^+-laden SGO/Fe-Mn, the decrease of thiol groups (decreased by 30.3% and 10.4%, respectively) can be attributed to surface complexation with mercury. The increase of sulfur oxides content (increased by 13.7% and 4.5%, respectively) indicated that some thiol groups were oxidized.

The XPS spectra of Si2p and Hg4f before and after mercury sorption are shown in Fig. 3M, N, and O. For Hg^{2+}/CH_3Hg^+-laden SGO/Fe-Mn, the peak spacing of $Hg4f_{5/2}$ and $Hg4f_{7/2}$ was 4.0 eV, and the binding energies of $Hg4f_{5/2}$ and $Hg4f_{7/2}$ were 104.9/105.4 and 100.9/101.4 eV, respectively, indicating mercury was adsorbed in an oxidized state of + II [45]. The intensity of $Hg4f_{5/2}$ in Hg^{2+}-laden SGO/Fe-Mn (Fig. 3N) was much stronger than that in CH_3Hg^+-laden SGO/Fe-Mn (Fig. 3O), which was due to the different mercury contents.

The FTIR, Raman, and XPS results demonstrated that the removal mechanisms of aqueous Hg^{2+} and CH_3Hg^+ can be described as ligand exchange and surface complexation with the sorption sites: −SH, −OH (including−OH derived from Fe-Mn oxides), O−C=O, C=C, Si−O groups, and π-π bond. Among them, −SH showed the strongest binding ability with mercury, forming sulfur-containing organic matter or polymers with Hg^{2+}, and sulfur-containing organometallic compounds and thiolate-like species with CH_3Hg^+. Meanwhile, during the sorption process, the surface charge distribution and electronegativity of SGO/Fe-Mn changed, and the redox reactions existed, resulting in a decrease in the surface negative charges of the material from -33.93 mV to -20.20 and -30.80 mV after reaction with Hg^{2+} and CH_3Hg^+, respectively.

3.2. Adsorption isotherm

Langmuir [46], Freundlich [47], BET [48], and SIPS [49] isotherm models are applied to fit the sorption isotherm data (Fig. 4), the resultant fitting parameters are summarized in Table S1 and S2. For Hg^{2+} sorption, the BET isotherm model (SGO/Fe-Mn: R^2 = 0.995; GO/Fe-Mn: R^2 = 0.996) outperformed the other three models. For CH_3Hg^+ sorption, BET isotherm model also fitted the best (SGO/Fe-Mn: R^2 = 0.997; GO/Fe-Mn: R^2 = 0.981).

The BET isotherm model describes a multi-layer adsorption process, assuming that the solid surface is homogeneous and multi-layer adsorption occurs, which can be expressed as:

$$q_e = q_m \frac{K_S C_e}{(1 - K_B C_e)(1 - K_B C_e + K_S C_e)} \quad (2)$$

where q_e is the uptake of mercury at equilibrium (mg/g), q_m is the maximum sorption capacity (mg/g), C_e is the equilibrium aqueous mercury concentration (mg/L), K_S is the equilibrium constant of sorption for 1 st layer (L/mg), K_B is the equilibrium constant of adsorption for upper layers (L/mg).

For the sorption of Hg^{2+} by SGO/Fe-Mn (Table S1), the K_S value was greater than K_B, i.e., 18.40 vs. 0.07 L/mg. K_S for SGO/Fe-Mn was larger than that for GO/Fe-Mn (18.40 vs. 2.26 L/mg), while the K_B values were similar (0.07 vs. 0.09 L/mg), which indicated that the 1 st layer sorption rate of Hg^{2+} was faster for SGO/Fe-Mn compared with GO/Fe-Mn, and there was little difference during upper layer sorption

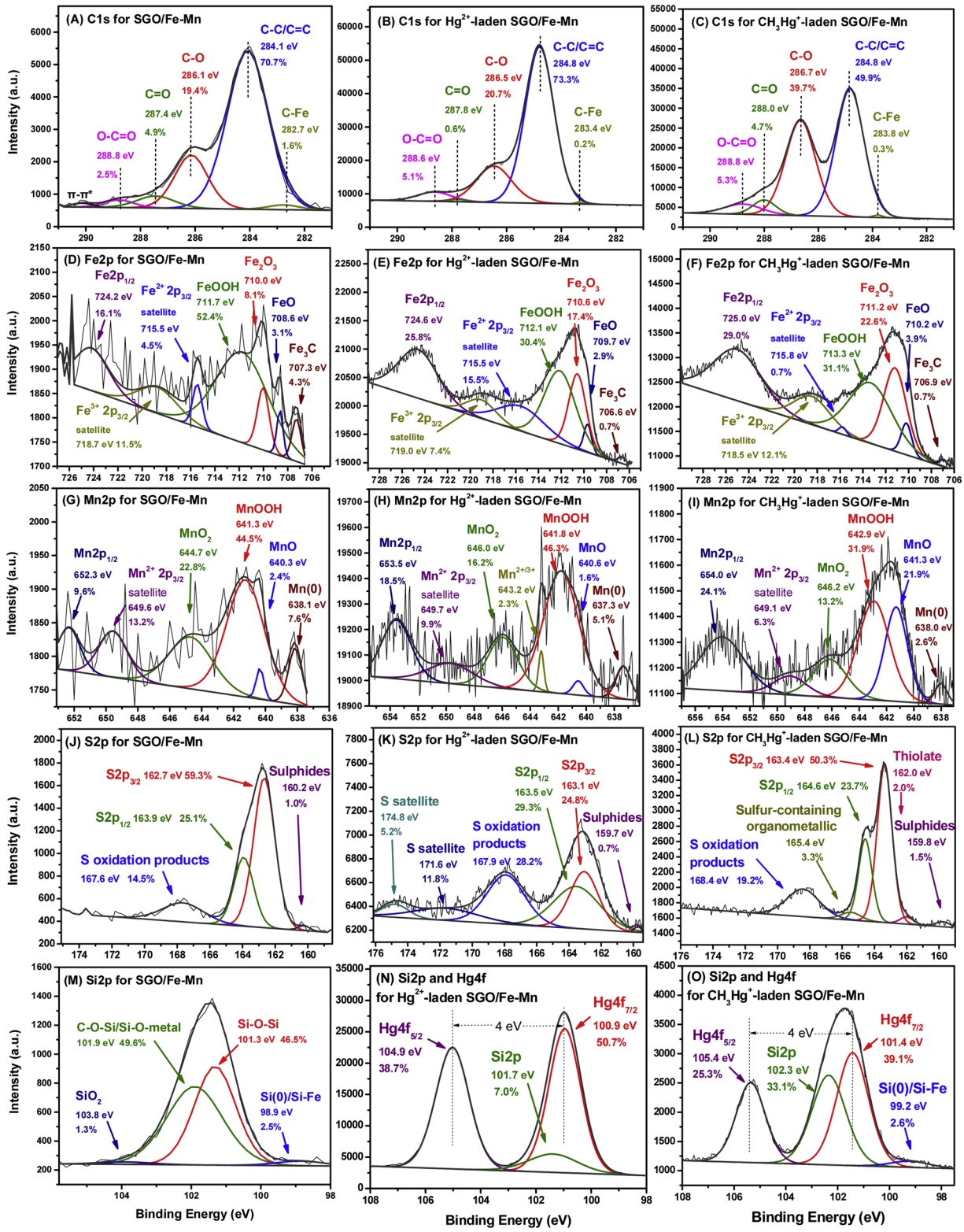

Fig. 3. XPS spectra of C1s (A, B, C), Fe2p (D, E, F), Mn2p (G, H, I), S2p (J, K, L), Si2p (M, N, O), and Hg4f (N, O) for SGO/Fe-Mn, Hg^{2+}-laden SGO/Fe-Mn and CH_3Hg^+-laden SGO/Fe-Mn, respectively.

process. The adsorption isotherm initially exhibited a very steep increase, which indicated high-energy adsorption sites (e.g., thiol group, oxygen-containing functional groups, and π-π band) [4]. As the active sites were gradually saturated, the single layer molecular sorption gradually transformed into multi-layer molecular adsorption.

The q_m of Hg^{2+} by SGO/Fe-Mn (233.17 ± 26.59 mg/g) was much higher than GO/Fe-Mn (42.39 ± 7.69 mg/g) and most reported thiol-functionalization materials, e.g., thiol-functionalized graphene oxide (107.5 mg/g) [5], thiol-functionalized mesoporous silica-coated magnetite nanoparticles (98.45-111.93 mg/g) [3], thiol-functionalized polymer-coated magnetic particles (84.25 mg/g) [10], thiol-rich polyhedral oligomeric silsesquioxane (12.9 mg/g) [7], thiol modified

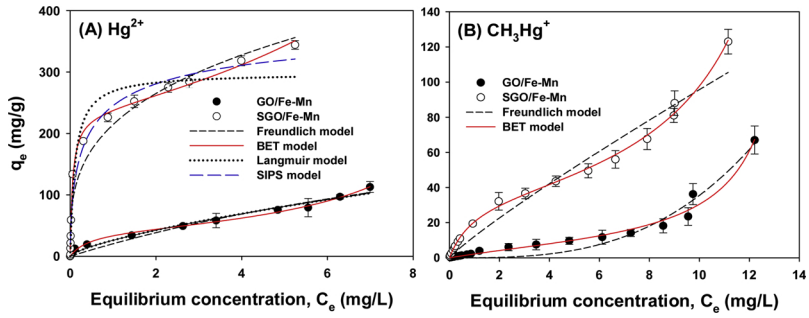

Fig. 4. (A) Hg^{2+} and (B) CH_3Hg^+ sorption isotherms via GO/Fe-Mn and SGO/Fe-Mn. 0.1–11 mg/L Hg^{2+}, 0.05–13 mg/L CH_3Hg^+. Adsorbent dosage 15 mg/L, pH 7.0 ± 0.2, 0.01 M $NaNO_3$, 3 days.

Fe_3O_4@SiO_2 (148.8 mg/g) [15], and thiol derivatized single wall carbon nanotubes (131 mg/g) [11].

SGO/Fe-Mn offered much greater q_m of CH_3Hg^+ (36.69 ± 3.90 mg/g) than GO/Fe-Mn (10.39 ± 4.59 mg/g) and most of reported materials, such as chitosan (0.006 mg/g) [50], barbital immobilized chitosan (0.01 mg/g) [50], glutaraldehyde cross-linked chitosan (0.0089 mg/g) [51], barbital-glutaraldehyde cross-linked chitosan (0.0072 mg/g) [51], *Coriandrum sativum* biosorbent (7 mg/g) [17], and *Lemna minor* powder (0.028 mg/g) [52].

At the initial stage of adsorption, the adsorption rate of monomolecular layer of CH_3Hg^+ was much slower than that of Hg^{2+} (K_S: 18.40 ± 1.88 for Hg^{2+} vs. 1.03 ± 0.11 L/mg for CH_3Hg^+), and the q_m of Hg^{2+} via SGO/Fe-Mn was higher than that of CH_3Hg^+ (233.17 ± 26.59 vs. 36.69 ± 3.90 mg/g). The difference of q_m and K_S values for Hg^{2+} and CH_3Hg^+ can be related to the difference of complex formation constants (log*K*) between thiol groups and mercury, i.e., RS-Hg (22.10) > RS-$HgCH_3$ (16.50) [53]. In addition, the constants (log*K*) for reactions with ligands are different, i.e., $Hg(OH)_2$ (21.83) > $HgOH^+$ (10.6) > MeHgOH (9.37) [19]. The value of K_S (1.03 ± 0.11 L/mg) was also higher than K_B (0.06 ± 0.05 L/mg) in the adsorption of CH_3Hg^+, i.e., the CH_3Hg^+ adsorption rate of single layer by SGO/Fe-Mn was also much higher than that of multilayer adsorption.

3.3. Effects of 3-MPTS content

As shown in Fig. 5, as the 3-MPTS content increased from 0 to 2%, and further to 6%, the q_e of Hg^{2+} (or CH_3Hg^+) was enhanced from 76.20 (or 0.17) to 173.20 (or 0.91) mg/g, and further to 197.52 (or 0.98) mg/g, respectively. The enhancement can be attributed to the increase of sulfur content in the SGO/Fe-Mn (from 0 to 3.84×10^{-3} and 5.41×10^{-3} mol/g) (Table S3). When the 3-MPTS content was further increased to 8%, the thiol content slightly decreased to 5.04×10^{-3} mol/g (Table S3), but both Hg^{2+} and CH_3Hg^+ remained

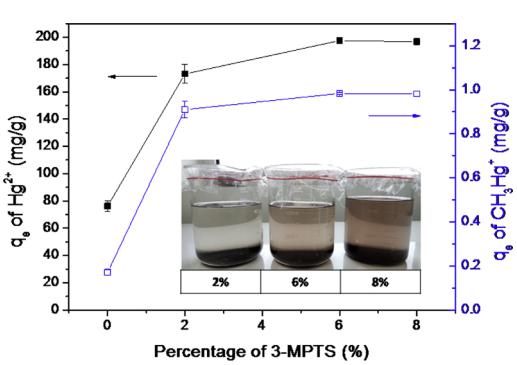

Fig. 5. Effects of 3-MPTS content on equilibrium uptake of Hg^{2+} and CH_3Hg^+ by SGO/Fe-Mn. 3 mg/L Hg^{2+} (adsorbent dosage 15 mg/L), 50 μg/L CH_3Hg^+ (adsorbent dosage 50 mg/L), pH 7.0 ± 0.2, 0.01 M $NaNO_3$, 3 days.

constant q_e. It should be noted that, increasing the content of 3-MPTS resulted in a gradual decrease of the Fe and Mn contents in SGO/Fe-Mn (Table S3), which presented a deeper reddish brown supernatant (Fig. 5). It is reported that 3-MPTS can combine with Fe-Mn oxides [9,14,15] and graphene oxide [5,16,17]. As the binding sites from Fe-Mn oxide decreased, more graphene oxide was exposed. While the lower sulfur content in 8% 3-MPTS (5.04×10^{-3} mol/g) compared to that in 6% 3-MPTS (5.41×10^{-3} mol/g) indicated that the loss outweighed the gain in the binding sites.

3.4. Effects of SGO/Fe-Mn dosage

Increasing the adsorbent dosage enhanced the mercury removal (Fig. S3). As shown in adsorption isotherm, the q_m of Hg^{2+} by SGO/Fe-Mn (or GO/Fe-Mn) was much larger than that of CH_3Hg^+, so the adsorbent dosage adopted was different. For Hg^{2+} adsorption (Fig. S3 A), when the adsorbent dosage was increased from 5 to 25 mg/L, the removal rate of Hg^{2+} was increased from 57.7% to 95.6% for SGO/Fe-Mn, and from 28.0% to 48.0% for GO/Fe-Mn, respectively. For CH_3Hg^+ sorption (Fig. S3B), as the SGO/Fe-Mn and GO/Fe-Mn dosage was increased from 30 to 70 mg/L, the removal rate was increased by 8.1% and 9.2%, respectively. An increase of adsorbent dosage resulted in more sorption sites.

3.5. Effects of pH

As the pH increased, the mercury uptake was increased first then decreased (Fig. 6). At low pH, H^+ and H_3O^+ might compete with Hg^{2+} or CH_3Hg^+ cations for surface sorption sites, and the adsorption sites derived from Fe-Mn oxides may be reduced. For SGO/Fe-Mn, the potential of zero charge was at pH < 3, as pH increased, the surface negative charge was increased, resulting in an increase of electrostatic attraction with mercury cations. For instance, the Hg^{2+} removal percentage rose from 73.4% to 90.2% as equilibrium pH increased from 3.8 to 6.0. At pH 3.0–5.5, SGO/Fe-Mn was negatively charged (Zeta potential was from -14.1 to -29.2 mV), Hg^{2+}, $HgOH^+$, and $Hg(OH)_2$ (aq) were the main forms of inorganic mercury (Fig. S4), CH_3Hg^+, CH_3HgCl (aq), and CH_3HgOH (aq) were the main forms of organic mercury [54]. Electrostatic attraction, cation-π interaction, ligand exchange, and surface complexation were the main removal mechanisms [4,24,53,54].

At pH > 5.5, uncharged $Hg(OH)_2$ (aq), CH_3HgCl (aq), and CH_3HgOH (aq) were the dominant forms of mercury, the bridges between functional groups might exist, electrostatic attraction and cation-π interaction were limited, resulting in a decrease of mercury uptake. For instance, the Hg^{2+} removal efficiency by SGO/Fe-Mn decreased from 90.2% to 78.0% as pH increased from 6.0 to 9.2. The changes for GO/Fe-Mn was more obvious owing to the lack of thiol groups. SGO/Fe-Mn maintained a stable and high mercury (Hg^{2+} and CH_3Hg^+) removal over a wider pH range of 4.5–8.0 than previously reported thiol-modified adsorbents, such as thiol-modified graphene oxide (performed well

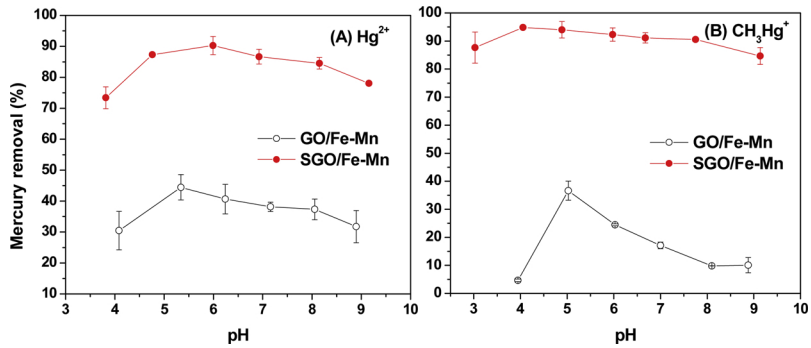

Fig. 6. Effects of pH on equilibrium uptake of (A) Hg^{2+} and (B) CH_3Hg^+. 3 mg/L Hg^{2+} (15 mg/L adsorbent), 50 μg/L CH_3Hg^+ (50 mg/L adsorbent), 0.01 M $NaNO_3$, 3 days.

at a pH range of 5.5–7.0) [5], thiol-modified activated carbon (pH range = 7.0–8.0) [6], and thiol-modified polymer-coated magnetic particles (pH range = 7.0–8.0) [10]. For thiol-modified single wall carbon nanotubes, the adsorption of mercury was continuously increased with the increase of pH from 1 to 9 [11].

3.6. Effects of ionic strength

The increase of ionic strength led to a slight decrease of mercury uptake (Fig. 7). For instance, following an increase of ionic strength from 0 to 0.1 M $NaNO_3$, the mercury removal by SGO/Fe-Mn decreased from 88.7% to 79.3% for Hg^{2+}, and from 98.8% to 86.0% for CH_3Hg^+, respectively. On one hand, $NaNO_3$ can screen the electrostatic interaction between sorbent and mercury, resulting in a change in the activity coefficient or the property of electrical double layer, limiting the mercury transfer onto adsorbent surface [55]. On the other hand, Na^+ may compete with mercury for the sorption sites. SGO/Fe-Mn demonstrated more stable mercury adsorption properties than some reported materials. For example, the Hg^{2+} removal by thiol-modified Fe_3O_4@SiO_2 was decreased by ~20% when ionic strength increased from 0 to 0.01 M [15], while the removal was only decreased by 1.7% for SGO/Fe-Mn in our study.

3.7. Effects of humic acid

As shown in Fig. 8, with the increase of humic acid from 0 to 25 mg/L, the removal rates of Hg^{2+} and CH_3Hg^+ by SGO/Fe-Mn were decreased from 86.6% to 42.7% and from 91.0% to 83.5%, respectively. Humic substances carry a large number of O—C═O groups and some other functional groups (e.g., —SH and —NH_2), which can not only bind with mercury (compete with adsorbents for mercury) and the sorption sites (e.g., hydroxyl) of adsorbent (occupy the adsorption sites), but also increase the mass transfer barrier for mercury uptake [56], resulting in a decreased mercury removal. CH_3Hg^+ has lower stability constants of the complex (lgK_n, n represents the number of ligands) than Hg^{2+} when it binds to ligands (e.g., thiol, hydroxyl, carboxyl, amino) in humic substances, as a result, humic acid demonstrated a greater impact on Hg^{2+} sorption than CH_3Hg^+ sorption.

It should be noted that the mercury removal by GO/Fe-Mn was enhanced by 16.0% for Hg^{2+} and 2.0% for CH_3Hg^+ when the humic acid increased from 0 to 4 mg/L (Fig. 8A), whereas the removal was decreased by 29.6% for Hg^{2+} and 12.6% for CH_3Hg^+ as humic acid further increased to 25 mg/L. The improvement in the mercury uptake might be related to the adsorption of humic acid onto SGO/Fe-Mn. Hg^{2+} and CH_3Hg^+ are reported to preferentially bind to thiol ligands (lgK_1, 22.1 and 16.5) rather than to hydroxyl (lgK_1, 10.6 and 9.4), carboxyl (lgK_1, 9.7 and 3.2), and amino ligands (lgK_1, 8.7 and 7.6) over the pH range of 0–14 [53,56]. As a result, the adsorbed humic acid which can provide thiol ligands on GO/Fe-Mn promoted the mercury uptake.

3.8. Desorption and regeneration

SGO/Fe-Mn was repeatedly used in three consecutive cycles of operation (cycle = adsorption + regeneration). Fig. 9A showed that 4 M KI effectively desorbed 85.3-80.0% of Hg^{2+} from Hg-laden SGO/Fe-Mn while 5% thiourea desorbed 32.0%-15.0% of Hg^{2+}. More than 95.0% of adsorbed CH_3Hg^+ was consistently desorbed by the desorbents 5% thiourea + 2 M KI, 2% thiourea + 4 M KI, and 5% thiourea + 4 M KI, respectively, much higher than by 5% thiourea (51.6-44.0%) and 4 M KI (84.8-80.0%) (Fig. 9B).

The samples after three consecutive sorption-regeneration cycles still had 98.1%, 96.7%, 98.8%, and 99.7% of original Hg^{2+} sorption capacity when 5% thiourea + 2 M KI, 5% thiourea + 4 M KI, 2% thiourea + 4 M KI, and 5% thiourea were used as the desorbing agents, respectively (Fig. 9C). The regenerated SGO/Fe-Mn had a more stable Hg^{2+} adsorption performance than some of the reported thiol-modified materials. For instance, after three regeneration cycles, the Hg^{2+}

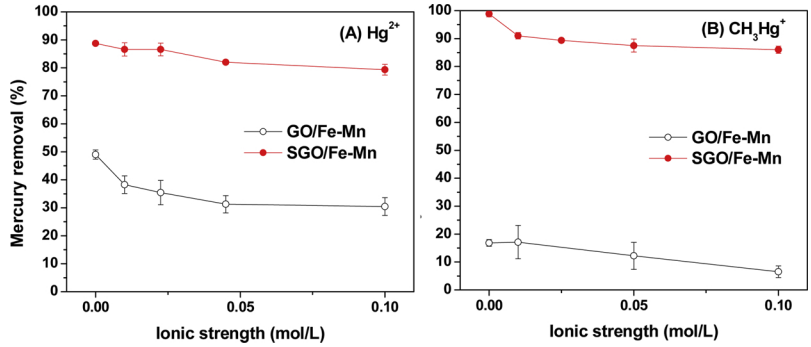

Fig. 7. Effects of ionic strength on equilibrium uptake of (A) Hg^{2+} and (B) CH_3Hg^+. 3 mg/L Hg^{2+} (15 mg/L adsorbent), 50 μg/L CH_3Hg^+ (50 mg/L adsorbent), pH 7.0 ± 0.2, 3 days.

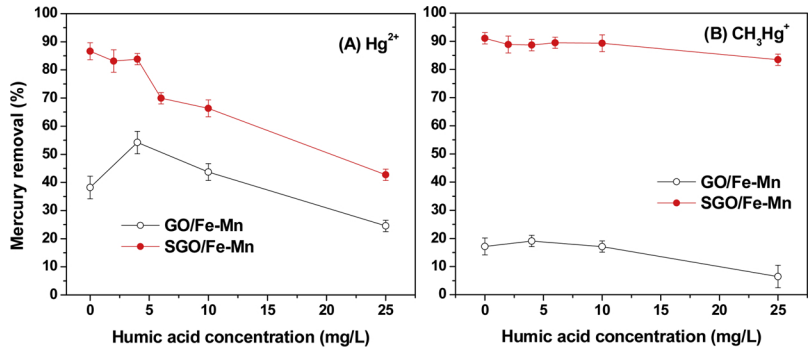

Fig. 8. Effects of humic acid on equilibrium uptake of (A) Hg^{2+} and (B) CH_3Hg^+. 3 mg/L Hg^{2+} (15 mg/L adsorbent), 50 μg/L CH_3Hg^+ (50 mg/L adsorbent), 0.01 M $NaNO_3$, 3 days.

sorption of thiol-modified Fe_3O_4@SiO_2 was decreased by ~26% [15], and thiol-modified single wall carbon nanotube was decreased by ~7% [11]. While the CH_3Hg^+ adsorption capacities by SGO/Fe-Mn progressively diminished with each cycle of regeneration (Fig. 9D). At the last regeneration cycle, it had 67.0%, 59.8%, 67.4%, 59.0, and 47.3% of the initial CH_3Hg^+ adsorption capacity as 5% thiourea + 2 M KI, 5% thiourea + 4 M KI, 2% thiourea + 4 M KI, 5% thiourea, and 4 M KI were used as the desorbing agents, respectively. The decrease of CH_3Hg^+ adsorption capacity may be related to the reduction of SGO/Fe-Mn by KI or thiourea.

Considering both the desorption and regeneration, the optimum desorbing agent used for Hg^{2+}- and CH_3Hg^+-laden SGO/Fe-Mn was 5% thiourea + 2 M KI. The results indicate that SGO/Fe-Mn has relatively good regenerability (especially for Hg^{2+} removal). Recovery of mercury and regeneration of SGO/Fe-Mn can realize the mercury resource utilization and minimize the operation cost.

3.9. Removal of Hg^{2+} in simulated waters via SGO/Fe-Mn and effects of coexisting heavy metals

The removal rates of Hg^{2+} via SGO/Fe-Mn in DI water, simulated surface water, simulated groundwater, and simulated seawater were 90.3%, 87.4%, 84.3%, and 20.7%, respectively (Fig. 10 A). The decrease of Hg^{2+} removal might be related to ionic strength. The sum of anions and cations were in the following order: DI water (0 M) < simulated surface water (9.76×10^{-4} M) < simulated groundwater (2.14×10^{-2} M) < simulated seawater (1.15 M). The high salinity of seawater inhibited the adsorption of Hg^{2+}, and the results were consistent with the "effect of the ionic strength" in this study. In other words, the SGO/Fe-Mn was more suitable for the remediation of mercury pollution in surface water and groundwater, not suitable for seawater. After adsorption, the decrease of pH (Fig. 10A) indicated the adsorption mechanism of ligand exchange.

In the presence of 3 mg/L of the coexisting heavy metals (Pb, Cu, Ni, Sb, Cd and Zn), the Hg^{2+} removal decreased from 90.3% to 80.8% (Fig.10 B), which indicated that SGO/Fe-Mn had high selectivity to mercury. And the decrease of mercury removal can be attributed to competitive adsorption (some adsorption sites were occupied). In addition, the SGO/Fe-Mn also had a certain selectivity for Pb and Cu (removal rates were 59.2%–82.6%), but has poor selectivity for Ni, Sb, Cd and Zn (removal rates were less than 20%).

4. Conclusions

SGO/Fe-Mn was successfully applied for the effective removal of aqueous Hg^{2+} and CH_3Hg^+. The BET sorption isotherm model well simulated the sorption isotherm data with a q_m of 233.17 mg/g for Hg^{2+} and 36.69 mg/g for CH_3Hg^+ by SGO/Fe-Mn, much higher than

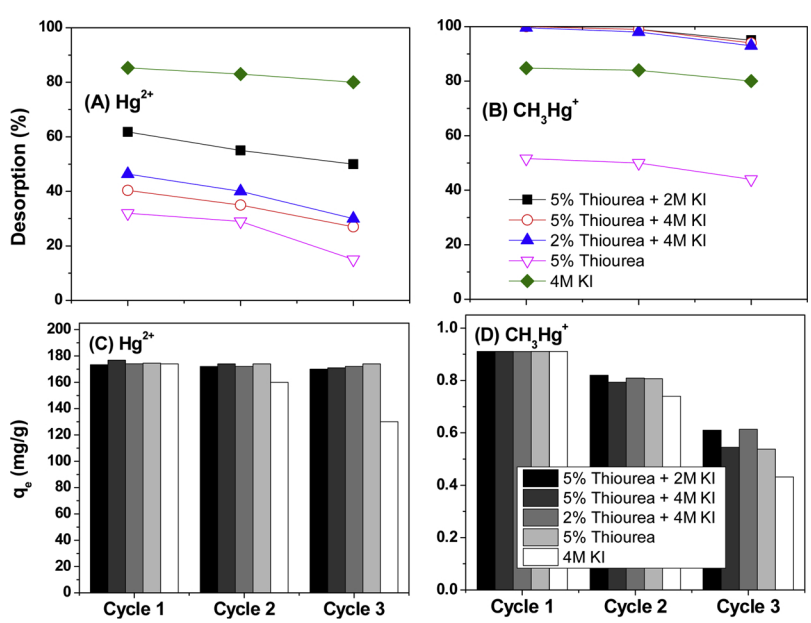

Fig. 9. (A, B) Desorption and (C, D) reuse of mercury-laden SGO/Fe-Mn. Sorption conditions: 0.01 M $NaNO_3$, pH 7.0 ± 0.2, 3 mg/L Hg^{2+} (15 mg/L SGO/Fe-Mn), 50 μg/L CH_3Hg^+ (50 mg/L SGO/Fe-Mn).

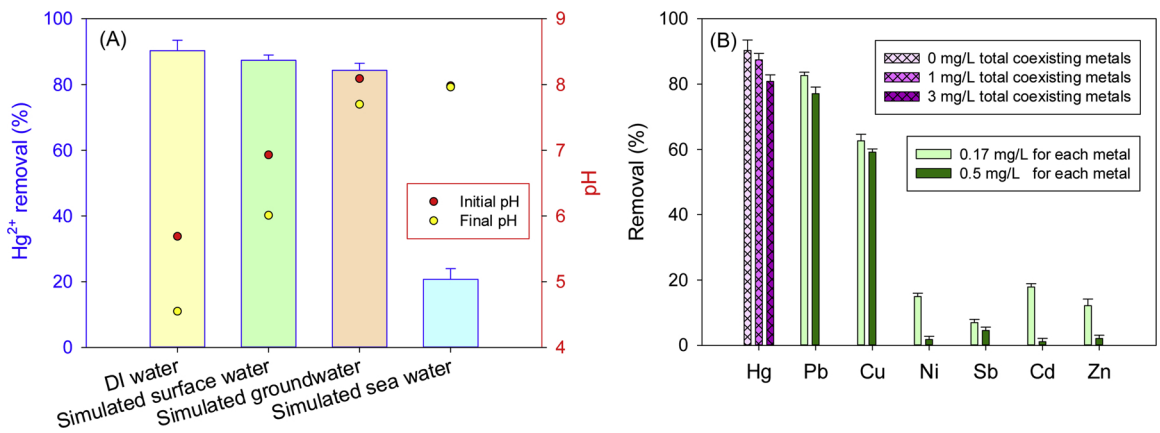

Fig. 10. (A) Removal of Hg^{2+} via SGO/Fe-Mn in simulated surface water, groundwater, and seawater and (B) effects of coexisting heavy metals (Pb, Cu, Ni, Sb, Cd and Zn) on Hg^{2+} removal by SGO/Fe-Mn. The concentration of Hg^{2+} was 3 mg/L, the total concentration of coexisting heavy metals was 0, 1 (each was 0.17 mg/L), and 3 mg/L (each was 0.5 mg/L), and pH = 6.00 ± 0.2.

that of GO/Fe-Mn (42.39 and 10.39 mg/g). Ligand exchange and surface complexation between Hg^{2+}/CH_3Hg^+ and surface active sites (i.e., −SH, −OH, O−C=O, C=C, Si−O, and π-π bond) were the dominant removal mechanisms. Among the active sites, −SH demonstrated the strongest binding ability with mercury, forming sulfur-containing organic matter or polymers with Hg^{2+}, and sulfur-containing organometallic compounds or thiolate-like species with CH_3Hg^+. Mercury uptake was enhanced with increasing 3-MPTS content, adsorbent dosage, and pH (< 5.5). Yet, the uptake was inhibited by high pH (> 5.5) and high concentrations of humic acid or electrolytes. Moreover, 5% thiourea + 2 M KI was the optimum desorbing agent for Hg^{2+}/CH_3Hg^+-laden SGO/Fe-Mn, the SGO/Fe-Mn can be successfully regenerated and reused for at least three times. The findings in this study indicate that SGO/Fe-Mn has high selectivity to mercury in the presence of Pb, Cu, Ni, Sb, Cd and Zn, and holds the promise to be employed as an effective sorbent for mercury remediation in surface water and groundwater.

Acknowledgements

The authors gratefully acknowledge the partial financial supports from National Natural Science Foundation of China (41503085, 41473070, and 41807115), the Fundamental Research Funds for the Central Universities, China, the Science and Technology Program of Guangzhou (No. 201804020050), the Guangdong Innovative and Entrepreneurial Research Team Program, China (No. 2016ZT06N569), Key Laboratory of Original Agro-Environmental Pollution Prevention and Control, Ministry of Agriculture/Tianjin Key Laboratory of Agro-environment and Safe-product (18nybcdhj-1), Tianjin S&T Program (17PTGCCX00240, 16YFXTSF00520, 17ZXSTXF00050), and 111 program, Ministry of Education, China (T2017002).

Appendix A. Supplementary data

Supplementary material related to this article can be found, in the online version, at doi:https://doi.org/10.1016/j.jhazmat.2018.11.074.

References

[1] P. Miretzky, A.F. Cirelli, Hg(II) removal from water by chitosan and chitosan derivatives: a review, J. Hazard. Mater. 167 (2009) 10–23.
[2] R.P. Mason, J.R. Reinfelder, F.M.M. Morel, Uptake, toxicity, and trophic transfer of mercury in a coastal diatom, Environ. Sci. Technol. 30 (1996) 1835–1845.
[3] O. Hakami, Y. Zhang, C.J. Banks, Thiol-functionalised mesoporous silica-coated magnetite nanoparticles for high efficiency removal and recovery of Hg from water, Water Res. 46 (2012) 3913–3922.
[4] Y. Huang, J. Tang, L. Gai, Y. Gong, H. Guan, R. He, H. Lyu, Different approaches for preparing a novel thiol-functionalized graphene oxide/Fe-Mn and its application for aqueous methylmercury removal, Chem. Eng. J. 319 (2017) 229–239.
[5] A.S. Krishna Kumar, S.-J. Jiang, W.-L. Tseng, Facile synthesis and characterization of thiol-functionalized graphene oxide as effective adsorbent for Hg(II), J. Environ. Chem. Eng. 4 (2016) 2052–2065.
[6] F. Kazemi, H. Younesi, A.A. Ghoreyshi, N. Bahramifar, A. Heidari, Thiol-incorporated activated carbon derived from fir wood sawdust as an efficient adsorbent for the removal of mercury ion: batch and fixed-bed column studies, Process Saf. Environ. Prot. 100 (2016) 22–35.
[7] W. Wang, M. Chen, X. Chen, J. Wang, Thiol-rich polyhedral oligomeric silsesquioxane as a novel adsorbent for mercury adsorption and speciation, Chem. Eng. J. 242 (2014) 62–68.
[8] K.-L. Fu, M.-Y. Yao, C.-g. Qin, G.-W. Cheng, Y. Li, M. Cai, S. Yang, J.-P. Nie, Study on the removal of oxidized mercury (Hg^{2+}) from flue gas by thiol chelating resin, Fuel Process. Technol. 148 (2016) 28–34.
[9] F. He, W. Wang, J.W. Moon, J. Howe, E.M. Pierce, L. Liang, Rapid removal of Hg(II) from aqueous solutions using thiol-functionalized Zn-doped biomagnetite particles, ACS Appl. Mater. Interfaces 4 (2012) 4373–4379.
[10] K. Jainae, N. Sukpirom, S. Fuangswasdi, F. Unob, Adsorption of Hg(II) from aqueous solutions by thiol-functionalized polymer-coated magnetic particles, J. Ind. Eng. Chem. 23 (2015) 273–278.
[11] N.M. Bandaru, N. Reta, H. Dalal, A.V. Ellis, J. Shapter, N.H. Voelcker, Enhanced adsorption of mercury ions on thiol derivatized single wall carbon nanotubes, J. Hazard. Mater. 261 (2013) 534–541.
[12] J.H. Richard, H. Biester, Mercury removal from contaminated groundwater: performance and limitations of amalgamation through brass shavings, Water Res. 99 (2016) 272–280.
[13] E.D. Morway, C.E. Thodal, M. Marvin-DiPasquale, Long-term trends of surface-water mercury and methylmercury concentrations downstream of historic mining within the Carson River watershed, Environ. Pollut. 229 (2017) 1006–1018.
[14] A. Guimarães, V. Ciminelli, W. Vasconcelos, Smectite organofunctionalized with thiol groups for adsorption of heavy metal ions, Appl. Clay Sci. 42 (2009) 410–414.
[15] S. Zhang, Y. Zhang, J. Liu, Q. Xu, H. Xiao, X. Wang, H. Xu, J. Zhou, Thiol modified Fe_3O_4@SiO_2 as a robust, high effective, and recycling magnetic sorbent for mercury removal, Chem. Eng. J. 226 (2013) 30–38.
[16] B. Yu, X. Wang, W. Xing, H. Yang, X. Wang, L. Song, Y. Hu, S. Lo, Enhanced thermal and mechanical properties of functionalized graphene/thiol-ene systems by photopolymerization technology, Chem. Eng. J. 228 (2013) 318–326.
[17] D. Karunasagar, M.V. Krishna, S.V. Rao, J. Arunachalam, Removal and preconcentration of inorganic and methyl mercury from aqueous media using a sorbent prepared from the plant Coriandrum sativum, J. Hazard. Mater. 118 (2005) 133–139.
[18] J. Tang, Y. Huang, Y. Gong, H. Lyu, Q. Wang, J. Ma, Preparation of a novel graphene oxide/Fe-Mn composite and its application for aqueous Hg(II) removal, J. Hazard. Mater. 316 (2016) 151–158.
[19] E. Tipping, Modelling the interactions of Hg(II) and methylmercury with humic substances using WHAM/Model VI, Appl. Geochem. 22 (2007) 1624–1635.
[20] J. Hedberg, M.T. Ekvall, L.-A. Hansson, T. Cedervall, I. Odnevall Wallinder, Tungsten carbide nanoparticles in simulated surface water with natural organic matter: dissolution, agglomeration, sedimentation and interaction with Daphnia magna, Environ. Sci.: Nano 4 (2017) 886–894.
[21] H. Dong, I.M.C. Lo, Transport of surface-modified nano zero-valent iron (SM-NZVI) in saturated porous media: effects of surface stabilizer type, subsurface geochemistry, and contaminant loading, Water Air Soil Pollut. 225 (2014) 2107.
[22] T. Zhao, Z. Liu, C. Du, C. Dai, X. Li, B. Zhang, Corrosion fatigue crack initiation and initial propagation mechanism of E690 steel in simulated seawater, Mater. Sci. Eng.: A 708 (2017) 181–192.
[23] H. Lyu, J. Tang, Y. Huang, L. Gai, E.Y. Zeng, K. Liber, Y. Gong, Removal of hexavalent chromium from aqueous solutions by a novel biochar supported nanoscale iron sulfide composite, Chem. Eng. J. 322 (2017) 516–524.
[24] D.A. Dougherty, The cation−π interaction, Acc. Chem. Res. 46 (2013) 885–893.

[25] P.N. Diagboya, B.I. Olu-Owolabi, D. Zhou, B.-H. Han, Graphene oxide-tripolyphosphate hybrid used as a potent sorbent for cationic dyes, Carbon 79 (2014) 174–182.
[26] X. Fu, F. Bei, X. Wang, S. O'Brien, J.R. Lombardi, Excitation profile of surface-enhanced Raman scattering in graphene-metal nanoparticle based derivatives, Nanoscale 2 (2010) 1461–1466.
[27] Y. Wang, X. Zou, W. Ren, W. Wang, E. Wang, Effect of silver nanoplates on Raman spectra of *p*-aminothiophenol assembled on smooth macroscopic gold and silver surface, J. Phys. Chem. C 111 (2007) 3259–3265.
[28] R. Graupner, Raman spectroscopy of covalently functionalized single-wall carbon nanotubes, J. Raman Spectrosc. 38 (2007) 673–683.
[29] H. Wang, J.T. Robinson, X. Li, H. Dai, Solvothermal reduction of chemically exfoliated graphene sheets, J. Am. Chem. Soc. 131 (2009) 9910–9911.
[30] H. Fu, D. Zhu, Graphene oxide-facilitated reduction of nitrobenzene in sulfide-containing aqueous solutions, Environ. Sci. Technol. 47 (2013) 4204–4210.
[31] T. Herranz, S. Rojas, M. Ojeda, F.J. Perez-Alonso, P. Terreros, K. Pirota, J.L.G. Fierro, Synthesis, structural features, and reactivity of Fe-Mn mixed oxides prepared by microemulsion, Chem. Mater. 18 (2006) 2364–2375.
[32] M.C. Biesinger, B.P. Payne, A.P. Grosvenor, L.W.M. Lau, A.R. Gerson, R.S.C. Smart, Resolving surface chemical states in XPS analysis of first row transition metals, oxides and hydroxides: Cr, Mn, Fe, Co and Ni, Appl. Surf. Sci. 257 (2011) 2717–2730.
[33] J. Li, J. Chen, Y. Yu, C. He, Fe-Mn-Ce/ceramic powder composite catalyst for highly volatile elemental mercury removal in simulated coal-fired flue gas, J. Ind. Eng. Chem. 25 (2015) 352–358.
[34] C.D. Wagner, W.M. Riggs, L.E. Davis, J.F. Moulder, G.E. Muilenberg, Handbook of X-Ray Photoelectron Spectroscopy, Perkin-Elmer Corporation Physical Electronics Division, 1979.
[35] S.-A. Wohlgemuth, F. Vilela, M.-M. Titirici, M. Antonietti, A one-pot hydrothermal synthesis of tunable dual heteroatom-doped carbon microspheres, Green Chem. 14 (2012) 741.
[36] Y. Huang, S. Xia, J. Lyu, J. Tang, Highly efficient removal of aqueous Hg^{2+} and CH_3Hg^+ by selective modification of biochar with 3-mercaptopropyltrimethoxysilane, Chem. Eng. J. (2018).
[37] B. Carriere, J.P. Deville, D. Brion, J. Escard, X-ray photoelectron study of some silicon-oxygen compounds, J. Electron Spectrosc. Relat. Phenom. 10 (1977) 85–91.
[38] M. Akizuki, Y. Nakai, T. Fujii, Y. Oshima, Kinetic analysis of a solid base-catalyzed reaction in sub- and supercritical water using aldol condensation with $Mg(OH)_2$ as a model, Ind. Eng. Chem. Res. 56 (2017) 12111–12118.
[39] J.E. Mangold, C.M. Park, H.M. Liljestrand, L.E. Katz, Surface complexation modeling of Hg(II) adsorption at the goethite/water interface using the charge distribution multi-site complexation (CD-MUSIC) model, J. Colloid Interface Sci. 418 (2014) 147–161.
[40] X. Lu, X. Huangfu, J. Ma, Removal of trace mercury(II) from aqueous solution by *in situ* formed Mn-Fe (hydr)oxides, J. Hazard. Mater. 280 (2014) 71–78.
[41] P. Thanabalasingam, W.F. Pickering, Sorption of mercury(II) by manganese(IV) oxide, Environ. Pollut., Ser. B 10 (1985) 115–128.
[42] J.A. Gardella, S.A. Ferguson, R.L. Chin, $\pi^* \longleftarrow \pi$ shakeup satellites for the analysis of structure and bonding in aromatic polymers by X-ray photoelectron spectroscopy, Appl. Spectrosc. 40 (1986) 224–232.
[43] C.-C. Su, J.W. Faller, Application of electron spectroscopy for chemical analysis to the study of ambidentate binding in sulfoxide complexes, Inorg. Chem. 13 (1974) 1734–1736.
[44] W.S.V. Kwan, L. Atanasoska, L.L. Miller, Oligoimide monolayers covalently attached to gold, Langmuir 7 (1991) 1419–1425.
[45] S. Yang, Y. Guo, N. Yan, Z. Qu, J. Xie, C. Yang, J. Jia, Capture of gaseous elemental mercury from flue gas using a magnetic and sulfur poisoning resistant sorbent Mn/γ-Fe_2O_3 at lower temperatures, J. Hazard. Mater. 186 (2011) 508–515.
[46] I. Langmuir, The adsorption of gases on plane surfaces of glass, mica and platinum, J. Am. Chem. Soc. 40 (1918) 1361–1403.
[47] H. Freundlich, Over the adsorption in solution, J. Chem. Phys. 57 (1906) 385–470.
[48] A. Ebadi, J.S. Soltan Mohammadzadeh, A. Khudiev, What is the correct form of BET isotherm for modeling liquid phase adsorption? Adsorption 15 (2009) 65–73.
[49] R. Sips, Combined form of Langmuir and Freundlich equations, J. Chem. Phys. 16 (1948) 490–495.
[50] S. Kushwaha, B. Sreedhar, P. Padmaja, Sorption of phenyl mercury, methyl mercury, and inorganic mercury onto chitosan and barbital immobilized chitosan: spectroscopic, potentiometric, kinetic, equilibrium, and selective desorption studies, J. Chem. Eng. Data 55 (2010) 4691–4698.
[51] S. Kushwaha, P.P. Sudhakar, Adsorption of mercury(II), methyl mercury(II) and phenyl mercury(II) on chitosan cross-linked with a barbital derivative, Carbohydr. Polym. 86 (2011) 1055–1062.
[52] S.X. Li, F.Y. Zheng, H. Yang, J.C. Ni, Thorough removal of inorganic and organic mercury from aqueous solutions by adsorption on Lemna minor powder, J. Hazard. Mater. 186 (2011) 423–429.
[53] U. Skyllberg, J. Qian, W. Frech, K. Xia, W.F. Bleam, Distribution of mercury, methyl mercury and organic sulphur species in soil, soil solution and stream of a boreal forest catchment, Biogeochemistry 64 (2003) 53–76.
[54] T. Karlsson, U. Skyllberg, Bonding of ppb levels of methyl mercury to reduced sulfur groups in soil organic matter, Environ. Sci. Technol. 37 (2003) 4912–4918.
[55] B.S. Inbaraj, J.S. Wang, J.F. Lu, F.Y. Siao, B.H. Chen, Adsorption of toxic mercury (II) by an extracellular biopolymer poly(gamma-glutamic acid), Bioresour. Technol. 100 (2009) 200–207.
[56] S.-J. Yoon, L.M. Diener, P.R. Bloom, E.A. Nater, W.F. Bleam, X-ray absorption studies of CH_3Hg^+-binding sites in humic substances, Geochim. Cosmochim. Acta 69 (2005) 1111–1121.